

# CHEMISTRY

---

## AN **ASIAN** JOURNAL

www.chemasianj.org

### Accepted Article

**Title:** Redox Responsive Fluorescent nanoparticles based on Diselenide-containing AIEgens for Cell imaging and Selective Cancer Therapy

**Authors:** Wenkun Han, Song Zhang, Jingyu Qian, Jianxu Zhang, Xuhang Wang, Zhigang Xie, Bin Xu, Yanqiu Han, and Wenjing Tian

This manuscript has been accepted after peer review and appears as an Accepted Article online prior to editing, proofing, and formal publication of the final Version of Record (VoR). This work is currently citable by using the Digital Object Identifier (DOI) given below. The VoR will be published online in Early View as soon as possible and may be different to this Accepted Article as a result of editing. Readers should obtain the VoR from the journal website shown below when it is published to ensure accuracy of information. The authors are responsible for the content of this Accepted Article.

**To be cited as:** *Chem. Asian J.* 10.1002/asia.201801527

**Link to VoR:** <http://dx.doi.org/10.1002/asia.201801527>

A Journal of



A sister journal of *Angewandte Chemie*  
and *Chemistry* – A European Journal

---

WILEY-VCH

# Redox Responsive Fluorescent nanoparticles based on Diselenide-containing AIEgens for Cell imaging and Selective Cancer Therapy

Wenkun Han,<sup>[a]</sup> Song Zhang,<sup>[a]</sup> Jingyu Qian,<sup>[a]</sup> Jianxu Zhang,<sup>[b]</sup> Xuanhang Wang,<sup>[a]</sup> Zhigang Xie,<sup>[b]</sup> Bin Xu,<sup>\*[a]</sup> Yanqiu Han,<sup>[c]</sup> and Wenjing Tian<sup>\*[a]</sup>

**Abstract:** A fluorescent molecule diselenide-containing 9, 10-distyrylanthracene (DSA) derivative (SeDSA) with aggregation induced emission (AIE) characteristic was successfully synthesized and SeDSA nanoparticles (NPs) were prepared through nanoprecipitation method. SeDSA could coassemble with the antitumor prodrug, diselenide-containing paclitaxel (SePTX) which could be obtained by precipitation, to form SeDSA-SePTX Co-NPs (Co-NPs). Molecular dynamics (MD) simulations reveal that the driving forces for the self-assembly behaviors of SeDSA NPs and SePTX NPs are  $\pi$ - $\pi$  interactions and hydrophobic interactions, respectively. While the driving forces for Co-NPs include hydrophobic interactions between SeDSA and SePTX,  $\pi$ - $\pi$  interactions between SeDSA molecules and hydrophobic interactions between SePTX molecules. Meanwhile, Se-Se bonds play a crucial role in balancing the intramolecular forces. These diselenide-containing nanoparticles (SeDSA NPs, SePTX NPs and Co-NPs) exhibit high stability in physiological conditions and excellent reduction-sensitivity under redox agent glutathione (GSH) because of the selenium-sulfur exchange reaction between diselenide and GSH. Both SeDSA NPs and Co-NPs show strong orange fluorescence emissions on the account of the AIE feature of SeDSA and they were easily internalized by HeLa and HepG2 cells. Distinctively, the Co-NPs combine the advantage of SeDSA and SePTX for cell imaging and antineoplastic activity and exhibit selectivity of cytotoxicities between neoplasia cells and normal cells. It highlights developing diselenide-containing AIEgens as a unique approach to prepare uniform and stable fluorescent nanoparticles for the application in cell imaging and tumor treatment.

## Introduction

Cancer is one of the most serious diseases which severely challenges the survival of people and results in several million deaths every year.<sup>[1]</sup> Fluorescence-based optical imaging has successfully been applied in clinical medicine and aroused

interests of researchers because it can provide a direct visual method for cancer diagnosis and better understanding of biological processes, metabolism and pharmacokinetics.<sup>[2]</sup> Over the past few decades, a variety of fluorescent agents have been proverbially explored and applied for bioimaging owing to their excellent merits, and organic fluorescent dyes with tunable absorption and emission wavelengths are one of the significant agents used in bioimaging.<sup>[3]</sup> However, traditional dyes often suffer from inherent aggregation-caused quenching (ACQ) effect leading to no or weak fluorescence emission in solid state or in aqueous media. More importantly, intrinsic drawbacks such as poor stability, small Stokes shift and poor biocompatibility have also impeded their further development for bioimaging.<sup>[4]</sup> Since the uncommon photophysical phenomenon aggregation induced emission (AIE) by Tang and coworkers, considerable AIE fluorogens (AIEgens) have been developed by worldwide research groups.<sup>[5]</sup> And many researchers proposed different methods to increase the water solubility of AIEgens for their applications in biology. For example, doping into the amphiphilic polymers or silica matrix to generate water-dispersible AIE nanoparticles;<sup>[6]</sup> functionalized with hydrophilic peptides or amphiphilic polymers to make AIEgens hydrophilic;<sup>[7]</sup> modified by polar groups or ions<sup>[8]</sup> such as quaternary ammonium salt, pyridinium salt and sulfonate to enhance their water solubility. For the treatment of cancer, chemotherapy using small molecular anticancer drugs is one of the most extensively used modalities and has achieved improved therapeutic effects in clinic.<sup>[9]</sup> Unfortunately, most anticancer drugs are poorly water-soluble resulting in poor bioavailability and undesired side effects.<sup>[10]</sup> To enhance the solubility and better therapeutic efficacy of hydrophobic drugs, the dimer-induced self-assembly of pure drugs has been explored by a crowd of researchers because most hydrophobic drugs could be assembled as nanocarrier-based drug delivery systems based on supramolecular interactions,<sup>[11]</sup> such as  $\pi$ - $\pi$  interactions, hydrophobic interactions and electrostatic interactions. The inserted linkers of dimers like disulfide bond or diselenide bond have been broadly investigated as reduction responsive groups because they could be cleaved under the high concentration of redox agents (like GSH).<sup>[12]</sup> According to literatures, there is a more reductive environment in tumors with several times higher GSH concentration than that in normal tumor tissue,<sup>[13]</sup> which have attracted researchers to fabricate reduction responsive drug delivery systems based on disulfide bond or diselenide bond.<sup>[14]</sup> Synchronously, the reduction responsive drug delivery systems could show ability for selective release of prodrugs between normal and tumor cells because of the higher concentration of redox agents in tumor cells. Compared with disulfide bond, the strength of diselenide bond is much weaker leading to more reductive sensitivity of diselenide bond linked molecules than disulfide-containing compounds theoretically.<sup>[15]</sup> According to the unique sensitivity of diselenide bond towards the intracellular reductive environment, numbers

[a] W. Han, S. Zhang, J. Qian, X. Wang, Prof. B. Xu, Prof. W. Tian  
State Key Laboratory of Supramolecular Structure and Materials  
Jilin University  
Changchun, Jilin 130012 (China)  
E-mail: xubin@jlu.edu.cn, wjtian@jlu.edu.cn

[b] J. Zhang, Prof. Z. Xie  
State Key Laboratory of Polymer Physics and Chemistry  
Changchun Institute of Applied Chemistry  
Chinese Academy of Sciences  
Changchun, Jilin 130022 (China)

[c] Y. Han  
Department of Neurology  
No.2 Hospital Jilin University  
Changchun 130041, (China)

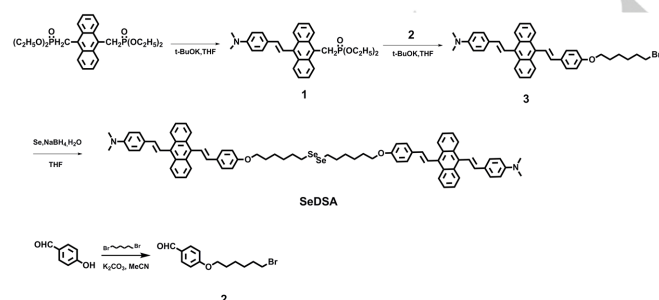
Supporting information for this article is given via a link at the end of the document.

of reductive sensitively diselenide-containing compounds have been tactfully utilized for drug delivery and cancer therapy. For instance, it has been reported that a serial of fluorescent dye dimers using S-S or Se-Se bond connect BODIPY dyes could self-assemble into nanoparticles for cell imaging and reduction responsive drug delivery systems; and a sequence of diselenide-containing polymers, including main chain and side chain block copolymers, dendrimers and hyperbranched polymers, could self-assemble and disassemble under various responsive stimuli for controlled drug delivery and enzyme mimics.<sup>[16]</sup>

Here, we introduced diselenide bond into 9, 10-distyrylanthracenederivative, a typical AIEgen to successfully synthesize SeDSA which could self-assemble into nanoparticles with enhanced fluorescence in aqueous suspension and co-assemble with diselenide-containing paclitaxel (SePTX), the antitumor prodrug, to form Co-NPs with dual functions of fluorescence cell imaging and antitumor activity.

## Results and Discussion

The molecular structure and synthetic route of SeDSA and SePTX were shown in Scheme S1. The required disodium diselenide ( $\text{Na}_2\text{Se}_2$ ) were synthesized through reduction of Se powder using  $\text{NaBH}_4$ .<sup>[17]</sup> Then the tetrahydrofuran (THF) solution of 3 was injected into the  $\text{Na}_2\text{Se}_2$  solution under  $\text{Ar}_2$  atmosphere. After the mixture solution was heated at 70 °C for 24h, the obtained SeDSA was measured and characterized by proton nuclear magnetic resonance ( $^1\text{H}$  NMR) and further confirmed by matrix-assisted laser desorption/ionization time-of-light mass spectrometry (MALDI-TOF), for which prominent signal at  $m/z=1208.081$  ( $m/z$  calcd: 1208.424) can be clearly observed. The diselenide-containing SePTX was obtained via the condensation reaction, and the compound were characterized by  $^1\text{H}$  NMR and MALDI-TOF mass spectrometry (Supporting Information, Figure S1).



**Scheme 1.** The synthetic route of SeDSA.

One simple and effective method to prepare small organic nanoparticles is reprecipitation means in aqueous solution.<sup>[18]</sup> The characterized SeDSA was dissolved in THF with drastic ultrasound, and then the uniform THF solution with SeDSA was added into deionized water tardily with vigorous stirring at room

temperature and then the mixture solution was dialyzed to remove the residual THF for 24h to form desired SeDSA NPs. SePTX could also self-assemble into SePTX NPs to form stable nanodrugs in water via nanoprecipitation method without any other auxiliary approaches. After carefully dialyzing to remove the remaining organic reagents, the acquired SePTX NPs were obtained. By means of the reprecipitation method, hydrophobic SeDSA and SePTX were dissolved in THF with sonication to gain a homogeneous mixture solution. After the solution with SeDSA and SePTX dropped into water with stirring, the obtained mixtures were dialyzed in water for 24h to get rid of the needless organic reagent so as to obtain the required SeDSA-SePTX NPs (Co-NPs). The concentration of the SeDSA was measured using a standard calibration curve technique by calculating the main absorbance of SeDSA at 426 nm through UV-Vis absorption spectra in THF/ $\text{H}_2\text{O}$  = 4:1 (Supporting Information, Figure S2). The final concentration of SeDSA in SeDSA NPs was 12.6  $\mu\text{g mL}^{-1}$ . The concentration of SePTX NPs was determined through high-performance liquid chromatography (HPLC, Shimadzu, CBM-20A) with an UV-vis detector using methanol: acetonitrile: water = 45: 45: 10 (v/v/v) as mobile phase. Similarly, concentrations of SePTX and SeDSA in Co-NPs were determined by HPLC and UV-vis absorption spectra. The final concentrations of SeDSA and SePTX in Co-NPs were 21 and 38  $\mu\text{g mL}^{-1}$ , respectively.

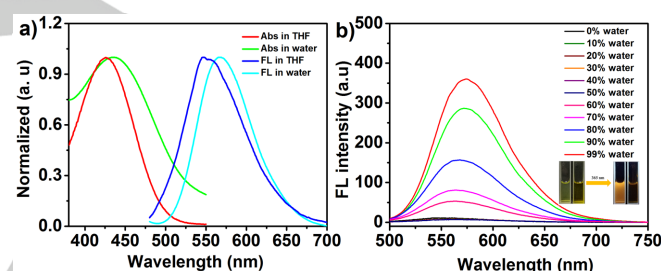


**Figure 1.** (a) Normalized UV-vis absorption and fluorescence spectra of SeDSA in THF and SeDSA NPs in water, respectively. (b) AIE property of SeDSA in THF-water mixtures with different water fractions. Inset in (b) are photos of SeDSA in THF:  $\text{H}_2\text{O}$  = 4:1 (v/v) solution (right) and SeDSA NPs in water (left) under natural light and UV 365 nm light.

We measured the UV-vis absorption and fluorescence spectra of SeDSA in THF and SeDSA NPs in water, respectively. As shown in Figure 1a, the maximum absorption of SeDSA in THF was at 426 nm and the main absorbance peak of SeDSA NPs in water was at 436 nm, which has 10 nm red-shift relative to that of SeDSA. The maximum fluorescence wavelength was centered at 548 nm for SeDSA in THF, but enhanced fluorescence was observed at 567 nm for SeDSA NPs due to the AIE feature of SeDSA.<sup>[19]</sup> As shown in Figure 1b, SeDSA NPs emitted strong orange fluorescence, while weak fluorescence was observed for SeDSA in THF. The fluorescence spectra of SeDSA in water and THF mixtures at different water fractions (fw) were carefully measured and the results are exhibited in Figure 1b. SeDSA is faintly fluorescence at 548 nm in its benign solvent (THF) because the molecularly dissolved

state can consume the energy through free molecular motion, which favors nonradiative decay.<sup>[20]</sup> However, with increasing water (poor solvent) fractions to 50%, SeDSA begins remarkable enhanced fluorescence emission, showing a characteristic of AIE. At 99% of fw, the fluorescence intensity at 572 nm is about 39-fold stronger than that in pure THF due to the formation of aggregates which restrict the intramolecular motion to activate the AIE process.<sup>[21]</sup> However, the fluorescence emission of SeDSA with different water fractions causes about 20 nm redshift, which is attributed to the intramolecular charge transfer (ICT) between nitrogen atom and DSA.

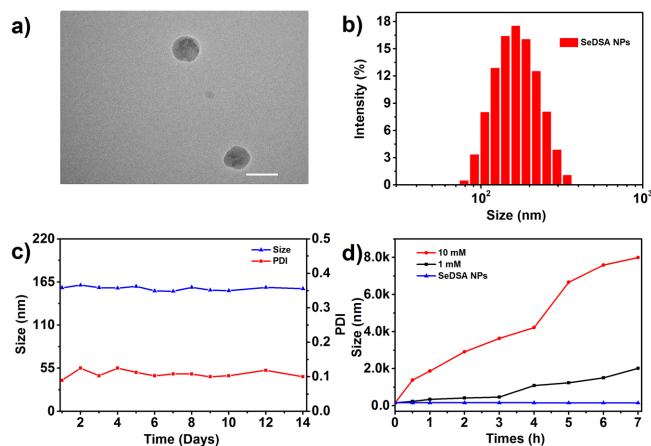


**Figure 2.** (a) TEM image of SeDSA NPs, scale bar: 200 nm. (b) DLS results of SeDSA NPs. (c) Changes of the SeDSA NPs and PDI as a function of time measured by DLS. (d) Size changes of SeDSA NPs over time determined by DLS in the presence of different concentrations of GSH.

The morphology and size distribution of SeDSA NPs, SePTX NPs and Co-NPs were characterized by transmission electronic microscopy (TEM) and dynamic light scattering (DLS) without further treatment. As shown in Figure 2, TEM measurement indicated that SeDSA NPs have uniform spherical structure and the hydrodynamic diameter with the average size of 157 nm was evaluated by DLS measurement, which was slightly larger than the value recorded by TEM. The initial polydispersity index (PDI) and zeta potential of SeDSA NPs are 0.133 and -30.8 mv. The TEM image and DLS measurements showed SeDSA could self-assemble into isolated nanoparticles in aqueous solution via nanoprecipitation method. The unchanged PDI and average sizes of SeDSA NPs after storing for 14 days indicated the SeDSA NPs have good stability in aqueous system which was also verified by TEM measurement (Supporting Information, Figure S3b). In addition, the slight changes of PDI and the size of SeDSA NPs after being incubated in phosphate buffer saline (PBS, pH 7.4) containing 10% fetal bovine serum (FBS) at 37 °C demonstrated the favorable stability of SeDSA NPs under physiological conditions (Supporting Information, Figure S3a). The SePTX NPs showed spherical morphology with the average size of 185.8 nm (Supporting Information, Figure S4a-c). TEM images showed that Co-NPs exhibited isolated spherical morphology with the average diameter of 190 nm, while the average diameter of hydrated Co-NPs was 242.5 nm and the

PDI was 0.134 with good size distribution. The SePTX NPs and Co-NPs also had excellent storage stability in water with no significant changes in the size for nearly half a month (Figure 3a-c, Figure S7a).

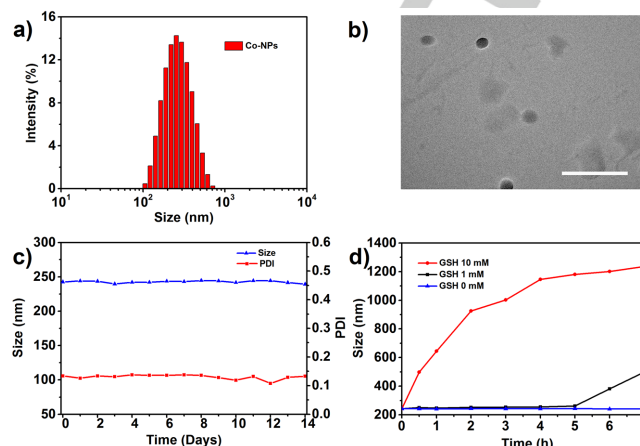


**Figure 3.** (a) DLS results of Co-NPs. Inside: Size, Z-Average and PDI of Co-NPs; (b) TEM image of Co-NPs, Scale bar: 1 μm; (c) Changes of the co-NPs and PDI as a function of time measured by DLS; (d) Size changes of co-NPs over time determined by DLS in the presence of different concentrations of GSH.

We further explored the self-assembling behaviors of SeDSA by molecular dynamics (MD) simulations<sup>[12]</sup>. SeDSA was initially arranged approximately vertical with an unmanipulated assembly process (Supporting Information, Figure S5A). After 10 ps in water, the final MD simulation position is shown in Figure S9A. The obtained data indicated that four SeDSA quickly flocked together to develop a cluster of tetramers and the conformation of SeDSA was slightly changed. As shown in Figure S5A, the two DSA derivatives of SeDSA are curved inside the cluster and  $\pi$ - $\pi$  interactions are found between DSA derivatives which are the main driving forces for the self-assembly behaviors of the SeDSA. Similarly, there are no direct interactions between Se-Se bonds. The dihedral angle (77.5°) between SeDSA planes in the self-assembled tetramers of SeDSA simulated by molecular dynamics (MD) (Supporting Information, Figure S5) and negative charge near Se-Se bond simulated by self-consistent reaction field (SCRf) method with the polarizable continuum model (PCM) (Supporting Information, Figure S10) indicated that Se-Se bond plays an indispensable role in balancing the intermolecular forces that control the self-assembly behaviors of SeDSA.<sup>[12]</sup> The inserted Se-Se bond also plays an indispensable role in balancing the intermolecular forces that control the self-assembly behaviors of SeDSA. However, when Se-Se bonds are broken, the segments of SeDSA NPs may form more energetically favorable conformations. Four SePTX rapidly aggregated into a cluster of tetramers inside which the PTX derivatives are curved and there are nonbonded hydrophobic interactions between SePTX. So the driving forces for the self-assembly of SePTX are nonbonded hydrophobic interactions. We further explored the co-assembling behaviours between SeDSA and SePTX by

molecular dynamics (MD) simulation method. As shown in Figure S5C, SeDSA and SePTX could come together to form a cluster of tetramers and there are strong  $\pi$ - $\pi$  interactions between SeDSA molecules and hydrophobic interactions between SePTX molecules. Considering the unique structure of the tetramer of Co-NPs, the driving forces for the co-assembly of Co-NPs are nonbonded hydrophobic interactions between SePTX and SeDSA.

### Redox Sensitivity

The diselenide-containing compounds could react with redox agent glutathione (GSH) *in vitro* and *in vivo* because of selenium-sulfur exchange reaction between diselenide bond and GSH.<sup>[22]</sup> So we explored the reduction-sensitivity of prepared SeDSA NPs *in vitro* using different concentrations of GSH to mimic the intracellular GSH level. SeDSA NPs were coped with 1mM and 10 mM GSH for different time at 37 °C and the control group was treated without redox agent GSH, then we monitored the size changes of SeDSA NPs by DLS for 7h. According to DLS results in Figure 2d, there were ignorable changes of the average size and PDI for SeDSA NPs after SeDSA NPs were incubated without reductive agents for 7h at 37 °C. Evident increase of the size (from 159 nm to 7986 nm), PDI ( from 0.133 to 1.00 ) and zeta potential (from -37.4 mv to 8.85 mv) for SeDSA NPs were observed when SeDSA NPs were incubated with 10 mM GSH at 37 °C for 7 h, indicating SeDSA NPs were reduction-sensitive under GSH. Moreover, large agglomerates of SeDSA exhibited bright orange fluorescent emission in Figure S6d because the disruption of diselenide bond under high concentration of GSH can make hydrophobic fragments of SeDSA aggregate into large agglomerates. Similarly, the reduction-sensitive behaviors of SeDSA NPs with 1 mM GSH were also detected by DLS. As displayed in Figure 2d, the average size of SeDSA NPs had an increase from 157 nm to 2022 nm after SeDSA NPs were treated with 1 mM GSH at 37 °C for 7 h. Furthermore, SeDSA NPs in serum containing solution with 10 mM GSH still possess efficient reductive behaviors. Figure S7b showed the size of SeDSA NPs increased from 220 nm to 1718 nm and obvious naked-visible suspension could be found under day light on the account of disassembly of SeDSA NPs with reduction agents, which demonstrated the efficient reductive behaviors of SeDSA NPs under physiological conditions. In order to explain why the PLQYs of SeDSA NPs and agglomerates were different, we first calculated the space occupancy of SeDSA and reduced monomer which are components of SeDSA NPs and agglomerates by using MD simulation. As shown in Fig. S11, the space occupancy of SeDSA was  $65.44 \pm 0.5$  %, while that of reduced monomer was  $66.24 \pm 0.4$ %. It means that SeDSA could aggregate into a little bit tighter structure in nanoparticles comparing with the reduced monomer in agglomerates, which should result in the enhanced emission of SeDSA nanoparticles due to the AIE characters of DSA derivative. Then we compared the self-assembly behaviors of SeDSA and reduced monomer (Supporting Information, Fig. S12) and found the  $\pi$ - $\pi$  interactions between DSA parts in SeDSA are stronger than

those in the reduced monomer, which means the fluorescence of SeDSA may be quenched by the strong  $\pi$ - $\pi$  interactions. Therefore, the relatively low space occupancy and strong  $\pi$ - $\pi$  interactions may cause the lower fluorescence quantum yield of SeDSA NPs than that of agglomerate. Also, we detected the reduction-sensitive behaviors of SePTX NPs in the presence of different concentrations of GSH *in vitro*. As Figure S4 shown, the particle sizes of SePTX NPs increased gradually under GSH, showing the nice reduction property of SePTX NPs (Supporting Information, Figure S4d). Meanwhile, the reduction properties of Co-NPs with 10 mM and 1 mM GSH were detected by DLS through tracking the changes of the diameters and PDI. As shown in Figure 3d, the diameter of Co-NPs increased from 242.5 nm to 1236 nm and PDI from 0.134 to 0.865 after being treated with 10 mM GSH for 7 h. And the size of Co-NPs could increase from 145.6 nm to 308.6 nm with 1mM GSH for 7 h. The continuous increase of size and PDI of Co-NPs with GSH demonstrated that Co-NPs are also reduction-sensitive.

### The cell uptake of SeDSA NPs and Co-NPs

We confirmed the biocompatibility of SeDSA NPs *in vitro* through measuring the cytotoxicity of SeDSA NPs toward HepG2 cells quantified by 3-(4, 5-dimethylthiazol-2-yl)-2, 5-diphenyl tetrazolium bromide (MTT) viability assay. As shown in Figure S8, after incubation at 37 °C with different concentrations of SeDSA NPs for 48 h, there were still 80% of cells survived with the concentration up to  $7.2 \mu\text{g mL}^{-1}$ , confirming the low cytotoxicity and good biocompatibility of SeDSA NPs *in vivo*. Flow cytometry was utilized to examine the quantitatively cellular uptake of the SeDSA NPs and Co-NPs. As shown in Figure S9a, it could be noticed that all internalization of the SeDSA NPs with increasing incubation time from 0.5 to 4 h, evidenced the time-dependent endocytosis.

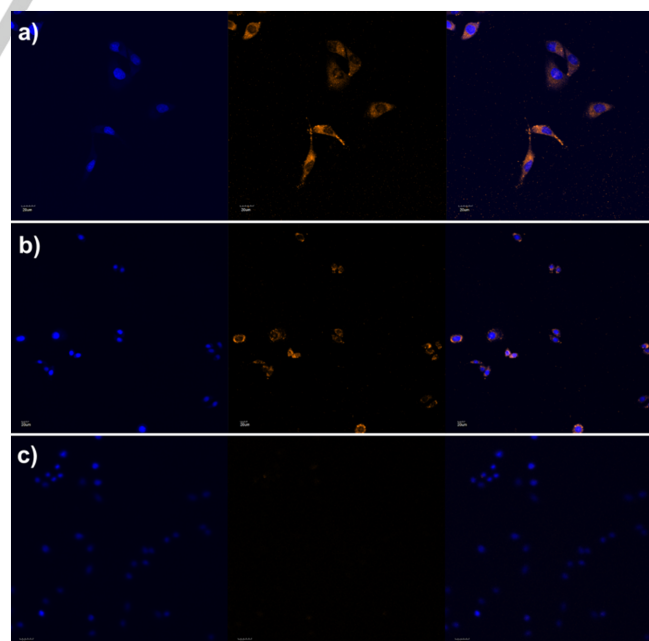


**Figure 4.** (a) CLSM images of (a) HeLa (b) HepG2 and (c) Skov 3 cells treated with SeDSA NPs for 2 h. For each panel, the images from left to right show cell nuclei stained by Hoechst (blue), SeDSA NPs fluorescence in cells (orange) and overlays of both images, scale bar : 20  $\mu\text{m}$ .

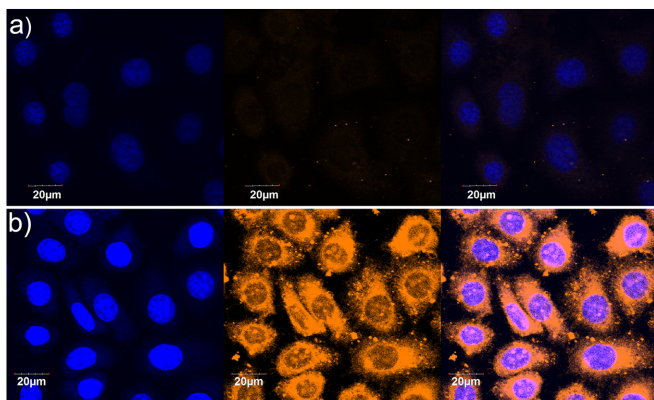


**Figure 5.** The representative CLSM images of HepG2 cells treated with Co-NPs for (a) 0.5 and (b) 2 h. For each panel, the images from left to right show cell nuclei stained by Hoechst (blue), SeDSA NPs fluorescence in cells (orange) and overlays of both images, scale bar : 20  $\mu\text{m}$ .

We used confocal laser scanning microscopy (CLSM) to investigate the cellular uptake of SeDSA NPs towards HepG2, HeLa and Skov 3. As shown in Figure 4, strong intracellular orange fluorescence was observed for HepG2 and HeLa cells after incubating with SeDSA NPs for 2 h, but there was weak fluorescence in Skov 3 cells evaluated by CLSM. It manifested that SeDSA NPs could be well internalized by HepG2 and HeLa cells. We further explored the reduction-response of SeDSA NPs in vitro by CLSM. HepG2 cells were first preprocessed with 1 mM N-ethylmaleimide (NEM) or 10 mM GSH for 15 min which could reduce or increase the concentrations of GSH in cells,<sup>[23]</sup> and then HepG2 cells were incubated with SeDSA NPs ( $0.87 \mu\text{g mL}^{-1}$ ) for 2 h in cell incubator at 37 °C. The control group only incubated with the same portion of SeDSA NPs without pretreatment. As shown in Figure 6, compared with the control group, HepG2 cells pretreated with GSH gave strong orange fluorescence emission and the group pretreated with NEM which could effectively quench biological thiol groups in the cytoplasm, gave weak orange fluorescence emission. The results indicated that the intracellular reducing agents like GSH could make a fast breaking of diselenide bond in SeDSA NPs.

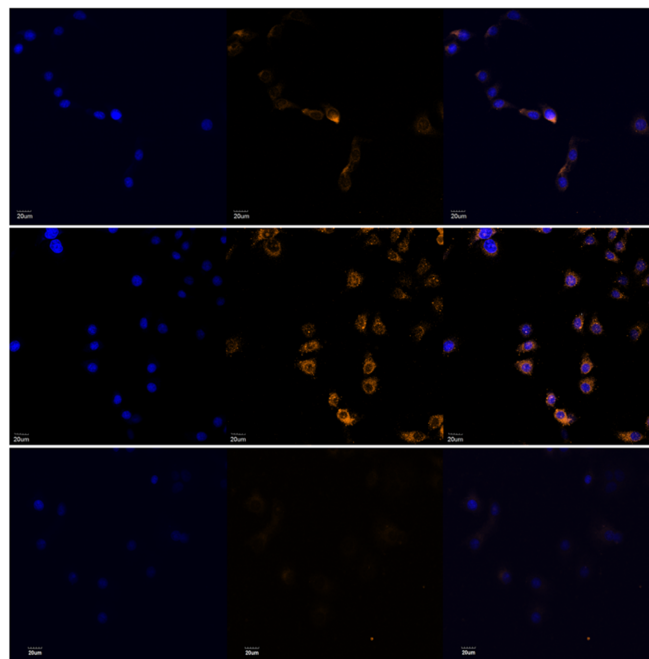


**Figure 6.** Confocal microscopy images of HepG2 cells, (a) without any pretreatment, and (b) pretreated with GSH (10 mM) for 15 min (c) pretreated with NEM (1 mM) for 15 min, then treated with SeDSA NPs ( $0.88 \mu\text{g mL}^{-1}$ ) for 2 h. For each panel, the images from left to right show cell nuclei stained by Hoechst (blue), SeDSA NPs fluorescence in cells (orange), and overlays of both images. Scale bar: 20  $\mu\text{m}$ .

We carried out the quantitatively cellular uptake of the Co-NPs using flow cytometry. The flow cytometry analysis (shown in Figure S9B) indicated that a significant increase in orange fluorescence intensity was detected after the HeLa cells were treated with Co-NPs for different time, identifying the time-dependent endocytosis for Co-NPs. To investigate the cellular uptake and further explore the potential of using of Co-NPs for bimolecular imaging in live cells, HepG2 cells were incubated with the same concentrations of Co-NPs for 0.5 h and 2 h in cell incubator. After staining the cell nuclei by Hoechst 33258, the cells were evaluated by CLSM. As shown in Figure 5, orange fluorescence was observed for the cells, indicating that Co-NPs could be endocytosed by HepG2 cells. In addition, the orange fluorescence intensity in HepG2 cells obviously increased in the wake of the increasing incubation time.

The cellular toxicity of Co-NPs toward the tumor cells (HeLa cells and HepG2 cells) and the normal cells (293T cells) was studied using MTT assays. Figure 7 showed that after 48 h incubation with different concentrations of free PTX and Co-NPs, Co-NPs have shown lower cytotoxicity than free PTX under the same concentration of PTX, which might ascribe the prompt diffusion of PTX into cytoplasm other than the endocytosis of Co-NPs. Surprisingly, we also found obvious cell cytotoxicities against tumor cells compared with normal cells. More than 70% of HepG2 cells and 50% of HeLa cells were killed at the concentration of  $5 \mu\text{g mL}^{-1}$  of PTX. In contrast, no more than 15% of 293T cells were killed, as shown in Figure 7. The  $\text{IC}_{50}$  values toward HeLa cells and HepG2 cells were  $3.96 \mu\text{g mL}^{-1}$  and

4.45 5  $\mu\text{g mL}^{-1}$ , which are lower than that of the normal cells ( $>5 \mu\text{g mL}^{-1}$ ) (Supporting Information, Table S1). These results manifested Co-NPs could distinguish the normal cells and tumor cells and kill the tumor cells selectively, due to the selenium-induced reactive oxygen species (ROS) in cancer cells causing the apoptosis.<sup>[12, 24]</sup>

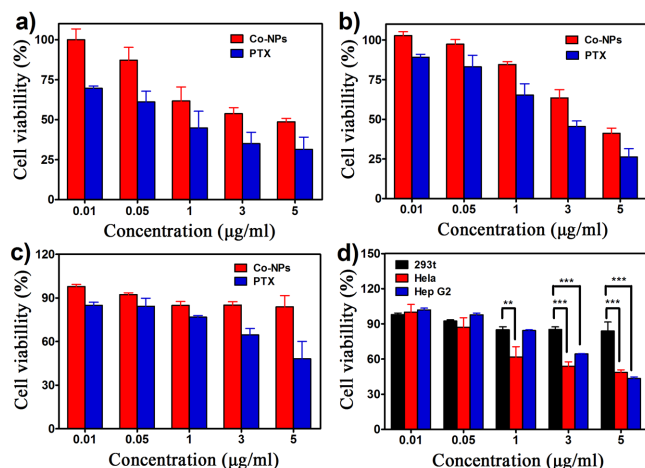


**Figure 7.** In vitro cytotoxicities of different concentrations of PTX and Co-NPs toward HepG2 (a) HeLa cells, (b) HepG2 cells, and (c) 239T cells incubated for 48 h. (d) Comparison of cytotoxicities in vitro toward tumor cells (HeLa and HepG2 cells) and normal cells (239T cells) after being incubated with Co-NPs for 48 h. Statistical significance analysis was assessed by SPSS via one-way ANOVA test; \*\* $P \leq 0.01$  was considered statistically highly significant; \*\*\* $P \leq 0.001$  was considered statistically highly significant.

## Conclusions

In summary, we successfully synthesized a novel fluorescent molecule SeDSA containing diselenide bond and AIEgens. SeDSA could self-assemble into uniform nanoparticles with orange fluorescence through usual nanoprecipitation method. Simultaneously, SeDSA and SePTX which is the reported diselenide-containing antitumor prodrug could coassemble into Co-NPs. The self-assembly driving forces of SeDSA NPs, SePTX NPs and Co-NPs explored by molecular dynamics (MD) simulations are  $\pi$ - $\pi$  interactions, hydrophobic interactions, and hydrophobic interactions between SeDSA and SePTX,  $\pi$ - $\pi$  interactions between SeDSA molecules and hydrophobic interactions between SePTX molecules, respectively. And there is indispensable contribution of the diselenide bond balancing the intermolecular forces. All the obtained nanoparticles linked by diselenide bond exhibited favorable stability in aqueous solution and physiological environment, which showed excellent redox sensitivity under the reductive environment with GSH. Because of the AIE property of SeDSA and the redox responsive property of diselenide bond, Co-NPs could be used for cell imaging and exerting the antitumor activity. The cytotoxicity experiments demonstrate that SeDSA NPs are biocompatible with low cytotoxicity and Co-NPs have lower cytotoxicity than free PTX under the same concentration of PTX,

and the results also revealed Co-NPs have an effect on selectivity treatment of tumor cells. So the redox responsive fluorescent nanoparticles based on diselenide-containing AIEgens show the potential applications in cell imaging and reduction-sensitive drug delivering.

## Experimental Section

### Material and instruments

Selenium powder, 1, 6-dibromohexane, 4-Hydroxybenzaldehyde and N-ethylmaleimide (NEM) were all purchased from Shanghai Energy Chemical. T-BuOK was purchased J&K Scientific Ltd, Glutathione (GSH) was purchased from Dingguo Biotech (Beijing, China), Sodium borohydride was purchased from Shanghai Macklin Biochemical Co., Ltd. Tetrahydrofuran (THF) and dichloromethane (DCM) were dried by distillation using sodium as drying agent and benzophenone as indicator. All non-aqueous reactions were carried out under argon atmosphere in oven-dried glassware. Milli-Q water (18.2 M $\Omega$ ) was used to prepare the buffer solutions from 1L PBS stock buffer. Unless otherwise indicated, all reagents were purchased from commercial available and used as received without further purification.  $^1\text{H}$  NMR spectra were measured in  $\text{CDCl}_3$  at room temperature by an AV-500 NMR spectrometer from Bruker. The average size, PDI and the zeta potential of the nanoparticles were recorded by Malvern Zeta-sizer Nano for dynamic light scattering (DLS). The DLS measurement was recorded at 25  $^\circ\text{C}$  and the scattering angle was fixed at 90 $^\circ$ . Transmission electron microscopy (TEM) was conducted by a JEM-2100F electron microscope. Matrix assisted laser desorption/ionization time-of light (MALDI-TOF) mass spectra (MS) were measured on a Bruker/Auto Reflex III mass spectrometer equipped (Bremen, Germany). UV-vis absorption spectra were conducted by a Shimadzu UV-2550 spectrophotometer. Fluorescence spectroscopy was taken with a Shimadzu RF-5301 PC spectrometer. Confocal laser scanning microscopy (CLSM) images were performed using an Olympus FV1000 confocal laser scanning microscope. Flow cytometry was obtained on Guava easyCyte 6-2L Base System (Merck Millipore, USA).

### Synthesis of the compound 2

4-Hydroxybenzaldehyde (2.44 g, 0.02 mol),  $\text{K}_2\text{CO}_3$  (5.52 g, 0.1 mol) were dissolved in 40 mL of  $\text{CH}_3\text{CN}$ , and then 1, 6-dibromohexane (16.6ml, 0.10 mol) was injected into the solution. The mixture solution was refluxed for 12 h. After filtration, the solvent was removed with a rotary evaporator and the residue was poured into 50 mL of water and extracted with  $\text{CH}_2\text{Cl}_2$ . The organic phase was collected, dried with  $\text{MgSO}_4$  and then the solvent was removed, the crude was further purified by flash column chromatography (dichloromethane/petroleum ether, 1:1 v/v) to afford 2 as a white solid.  $^1\text{H}$  NMR (500 MHz,  $\text{CDCl}_3$ )  $\delta$  9.90 (s, 1H), 7.85 (d,  $J = 8.6$  Hz, 2H), 7.01 (d,  $J = 8.6$  Hz, 2H), 4.07 (t,  $J = 6.4$  Hz, 2H), 3.45 (t,  $J = 6.7$  Hz, 2H), 1.89 (dp,  $J = 26.6, 6.6$  Hz, 4H), 1.66-1.45 (m, 4H).

### Synthesis of the compound 3

Compound 1 (236.8 mg, 0.5 mmol) and compound 2 (154.5 mg, 0.6 mmol) were dissolved in 20 ml dry THF under  $\text{N}_2$  with stirring, and t-BuOK (67.3 mg, 0.6 mmol) in 10 mL dry THF was added into the solvent under ice water bath. After the mixture stirred at room temperature for 24 h, the reaction mixture was quenched with 5 mL water, and then the solvent was removed with a rotary evaporator and the residue was poured into 50 mL of  $\text{CH}_2\text{Cl}_2$  and 50 mL brine, extracted with  $\text{CH}_2\text{Cl}_2$  (50

ml) three times. The organic phase was dried over  $\text{MgSO}_4$ , filtered and the filtrate was concentrated and purified by chromatography (dichloromethane/petroleum ether, 2: 1 v/v) to give compound 3 as an orange solid.

### Synthesis of SeDSA

Se powder (16 mg, 0.1 mmol) was dispersed in deionized water (2 mL) under the sonication in  $\text{Ar}_2$  and sodium borohydride (7.6 mg, 0.2 mmol) were also dissolved in deionized water (2 mL) during the sonication. The sodium borohydride solvent was slowly injected into the Se dispersion solution with stirring accompanying bubbling till the Se suspension liquid became a colorless solution. After the reaction mixture was heated at 70 °C for 30 min, the dark wine solution indicated the  $\text{Na}_2\text{Se}_2$  was obtained. Compound 3 (120 mg, 0.2 mmol) in 10 mL dry THF was injected into the dark wine solution. The reaction was performed at 70 °C for 14 h, and then the product was extracted with dichloromethane and dried with anhydrous  $\text{MgSO}_4$ . After evaporation, the crude product was purified by a silica gel column (dichloromethane/petroleum ether, 2: 1, v/v).  $^1\text{H}$  NMR (500 MHz,  $\text{CDCl}_3$ )  $\delta$  8.37 (dd,  $J = 6.4, 3.7$  Hz, 8H), 7.75 (d,  $J = 16.4$  Hz, 4H), 7.60 (t,  $J = 8.7$  Hz, 8H), 7.48 – 7.41 (m, 8H), 7.26 (s, 4H), 7.00 – 6.96 (m, 4H), 6.85 (d,  $J = 16.4$  Hz, 4H), 4.03 (t,  $J = 6.4$  Hz, 4H), 3.07 (s, 12H), 2.97 (t,  $J = 7.4$  Hz, 4H), 1.90 – 1.77 (m, 8H), 1.58–1.50 (m, 8H). MALDI-TOF:  $m/z$ : calcd. for  $(\text{C}_{76}\text{H}_{76}\text{N}_2\text{O}_2\text{Se}_2)$ :  $[\text{M}]^+$ : 1208.424; found:  $m/z$  1208.081.

### Acknowledgements

This work was supported by the Natural Science Foundation of China (21835001, 51773080, 21674041, 51573068, 21221063), Program for Changbaishan Scholars of Jilin Province, Jilin Province project (20160101305JC), and the “Talents Cultivation Program” of Jilin University.

### Conflict of interest

The authors declare no conflict of interest.

**Keywords:** diselenide bond • AIEgens • self-assembly • bioimaging • drug delivery

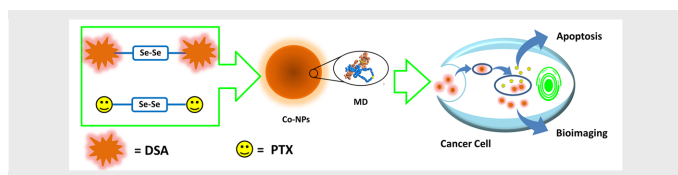
- [1] D. Cai; W. Gao, B. He, W. Dai, H. Zhang, X. Wang, J. Wang, X. Zhang, Q. Zhang, *Biomaterials* **2014**, *35*, 2283-2294.
- [2] a) E. Betzig, G. H. Patterson, R. Sougrat, O. W. Lindwasser, S. Olenych, J. S. Bonifacino, M. W. Davidson, J. Lippincott Schwartz and H. F. Hess, *Science* **2006**, *313*, 1642-1645; b) X. Feng, L. Liu, S. Wang D. Zhu, *Chem. Soc. Rev.* **2010**, *39*, 2411-2419; c) G. Sun, M. Y. Berezin, J. Fan, H. Lee, J. Ma, K. Zhang, K. L. Wooley, S. Achilefu, *Nanoscale* **2010**, *2*, 548-558.
- [3] a) V. Sokolova and M. Eppe, *Nanoscale* **2011**, *3*, 1957-1962; b) K. Uno, T. Sasaki, N. Sugimoto, H. Ito, T. Nishihara, S. Hagihara, T. Higashiyama, N. Sasaki, Y. Sato, K. Itami, *Chem. Asian J.* **2017**, *12*, 233-238; c) S. Mulay, T. Yudhistira, M. Choi, Y. Kim, J. Kim, Y.-J. Jang, S. Jon, D. -G. Churchill, *Chem. Asian J.* **2016**, *11*, 3598-3605; d) Y. Li, W. Liu, H. Zhang, M. Wang, J. Wu, J. Ge, P. Wang, *Chem. Asian J.* **2017**, *12*, 2098-2103; e) Y. Zhao, C. Shi, X. Yang, B. Shen, Y. Sun, Y. Chen, X. Xu, H. Sun, K. Yu, B. Yang, Q. Lin, *ACS Nano* **2016**, *10*, 5856-5863; f) W. Cheng, H. Cheng, S. Wan, X. Zhang, and M. Yin, *Chem. Mater.* **2017**, *29*, 4218-4226; g) S. Zhang, J. Li, J. Wei, M. Yin, *Science Bulletin* **2018**, *63*, 101-107.
- [4] R. Deans, J. Kim, M. R. Machacek, T. M. Swager, *J. Am. Chem. Soc.*, **2000**, *122*, 8565-8566.
- [5] a) J. Luo, Z. Xie, J. W. Y. Lam, L. Cheng, H. Chen, C. Qiu, H. S. Kwok, X. Zhan, Y. Liu, D. Zhu, B. Z. Tang, *Chem. Commun.* **2001**, *37*, 1740-1741; b) R. T. K. Kwok, C. W. T. Leung, J. W. Y. Lam, B. Z. Tang, *Chem. Soc. Rev.* **2015**, *44*, 4228-4238.
- [6] a) Z. Wang, L. Yan, L. Zhang, Y. Chen, H. Li, J. Zhang, Y. Zhang, X. Li, B. Xu, X. Fu, Z. Sun, W. Tian, *Polym. Chem.* **2014**, *5*, 7013-7020; b) X. Zhang, X. Zhang, B. Yang, L. Liu, J. Hui, M. Liu, Y. Chen, Y. Wei, *RSC Adv.* **2014**, *4*, 10060-10066; c) D. Li, J. Yu, *Small* **2016**, *47*, 6478-6494; d) W. Wu, D. Mao, F. Hu, S. Xu, C. Chen, C. -J. Zhang, X. Cheng, Y. Yuan, D. Ding, D. Kong, B. Liu, *Adv. Mater.* **2017**, *29*, 1700548; e) X. Zhang, X. Zhang, S. Wang, M. Liu, Y. Zhang, L. Tao, Y. Wei, *ACS Appl. Mater. Interfaces.* **2013**, *5*, 1943-1947.
- [7] a) Y. Yuan, C.-J. Zhang, R. T. K. Kwok, S. Xu, R. Zhang, J. Wu, B. Z. Tang, B. Liu, *Adv. Funct. Mater.* **2015**, *25*, 6586-6595; b) H. Li, X. Zhang, X. Zhang, B. Yang, Y. Yang, Z. Huang, Y. Wei, *RSC Adv.* **2014**, *4*, 21588-21592; c) Y. Zhang, Y. Chen, X. Li, J. Zhang, J. Chen, B. Xu, X. Fu, W. Tian, *Polym. Chem.* **2014**, *5*, 3824-3830; e) A. Han, H. Wang, R. T. K. Kwok, S. Ji, J. Li, D. Kong, B. Z. Tang, B. Liu, Z. Yang, D. Ding, *Anal. Chem.* **2016**, *88*, 3872-3878.
- [8] a) Y. Yuan, S. Xu, X. Cheng, X. Cai, B. Liu, *Angew. Chem. Int. Ed.* **2016**, *55*, 6457-6461; b) D. Wang, H. Su, R. T. K. Kwok, X. Hu, H. Zou, Q. Luo, M. M. S. Lee, W. Xu, J. W. Y. Lam, B. Z. Tang, *Chem. Sci.* **2018**, *9*, 3685-3693.
- [9] a) J. Zhang, S. Li, F. -F. An, J. Liu, S. Jin, J. -C. Zhang, P. C. Wang, X. Zhang, C. -S. Lee, X. -J. Liang, *Nanoscale*, **2015**, *7*, 13503-13510;
- [10] a) X. Wu, X. Sun, Z. Guo, J. Tang, Y. Shen, T. D. James, H. Tian, W. Zhu, *J. Am. Chem. Soc.* **2014**, *136*, 3579; b) J. H. Atkins, L. J. Gershell, *Nat. Rev. Cancer*, **2002**, *2*, 645.
- [11] a) D. He, W. Zhang, H. Deng, S. Huo, Y. -F. Wang, N. Gong, L. Deng, X. -J. Liang, A. Dong, *Chem. Commun.* **2016**, *52*, 14145-14148; b) Q. Song, X. Wang, Y. Wang, Y. Liang, Y. Zhou, X. Song, B. He, H. Zhang, W. Dai, X. Wang, Q. Zhang, *Mol. Pharmaceutics* **2016**, *13*, 190-201; c) H. Kasai, T. Murakami, Y. Ikuta, Y. Koseki, K. Baba, H. Oikawa, H. Nakanishi, M. Okada, M. Shoji, M. Ueda, H. Imahori, M. Hashida, *Angew. Chem. Int. Ed.* **2012**, *51*, 10315-10318; D) Y. Ma, Q. Mou, X. Zhu, D. Yan, *Materials Today Chemistry* **2017**, *4*, 26-39.
- [12] a) Y. Wang, D. Liu, Q. Zheng, Q. Zhao, H. Zhang, Y. Ma, J. K. Fallon, Q. Fu, M. T. Haynes, G. Lin, R. Zhang, D. Wang, X. Yang, L. Zhao, Z. He, F. Liu, *Nano Lett.* **2014**, *14*, 5577-5583; b) Q. Pei, X. Hua, S. Liu, Y. Li, Z. Xie, X. Jing, *Journal of Controlled Release* **2017**, *254*, 23-33; c) W. Zhang, W. Lin, Q. Pei, X. Hu, Z. Xie, X. Jing, *Chem. Mater.* **2016**, *28*, 4440-4446.
- [13] Y. -C. Wang, Y. Li, T. -M. Sun, M. -H. Xiong, J. Wu, Y. -Y. Yang, J. Wang, *Macromol. Rapid Commun.* **2010**, *31*, 1201-1206.
- [14] a) C. Sun, S. Ji, F. Li, H. Xu, *ACS Appl. Mater. Interfaces* **2017**, *9*, 12924-12929; b) X. Zheng, L. Wang, S. Liu, W. Zhang, F. Liu, Z. Xie, *Adv. Funct. Mater.* **2018**, *28*, 1706507.
- [15] a) K. N. K. J., *Chem. Educ.* **1995**, *72*, 423-424; b) H. J. Reich, R. J. Hondal, *ACS Chem. Biol.* **2016**, *11*, 821-841.
- [16] J. Xia, F. Li, S. Ji, H. Xu, *ACS Appl. Mater. Interfaces* **2017**, *9*, 21413-21421; b) W. Zhou, L. Wang, F. Li, W. Zhang, W. Huang, F. Huo, H. Xu, *Adv. Funct. Mater.* **2017**, *27*, 1605465; c) H. Xu, W. Cao, X. Zhang, *Acc. Chem. Res.* **2013**, *46*, 1647-1658.
- [17] D. L. Klayman, T. S. Griffin, *J. Am. Chem. Soc.* **1973**, *95*, 197-199.
- [18] L. Yan, Y. Zhang, B. Xu, W. Tian, *Nanoscale*, **2016**, *8*, 2471-2487.
- [19] X. Zhang, X. Zhang, B. Yang, L. Liu, J. Hui, M. Liu, Y. Chen, Y. Wei, *RSC Adv.* **2014**, *4*, 10060-10066.
- [20] J. Zhang, S. Ma, H. Fang, B. Xu, H. Sun, I. Chan, W. Tian, *Mater. Chem. Front.* **2017**, *1*, 1422-1429.
- [21] J. Mei, N. L. C. Leung, R. T. K. Kwok, J. W. Y. Lam, B. Z. Tang, *Chem. Rev.* **2015**, *115*, 11718-11940.
- [22] a) X. Han, X. Song, F. Yu, L. Chen, *Chem. Sci.* **2017**, *8*, 6991-7002; b) X. Han, X. Song, F. Yu, L. Chen, *Adv. Funct. Mater.* **2017**, *27*, 1700769,

For internal use, please do not delete. Submitted Manuscript

- c) M. Gao, F. Yu, C. Lv, J. Chood, L. Chen, *Chem. Soc. Rev.* **2017**, *46*, 2237-2271.
- [23] a) J. Ding, F. Shi, C. Xiao, L. Lin, L. Chen, C. He, X. Zhuang, X. Chen, *Polym. Chem.* **2011**, *2*, 2857-2864; b) M. H. Lee, J. H. Han, P. -S. Kwon, S. Bhuniya, J. Y. Kim, J. L. Sessler, C. Kang, J. S. Kim, *J. Am. Chem. Soc.* **2012**, *134*, 1316-1322.
- [24] K. Han, Q. Lei, S. B. Wang, J. J. Hu, W. X. Qiu, J. Y. Zhu, W. N. Yin, X. Luo, X. Z. Zhang, *Adv. Funct. Mater.* **2015**, *25*, 2961-2971 ; b) L. Zeng, L. Li, T. Li, W. Cao, Y. Yi, W. Geng, Z. Sun, H. Xu, *Chem. Asian J.* **2014**, *9*, 2295-2302.

WILEY-VCH

Accepted Manuscript

*Wenkun Han, Bin Xu\*, Wenjing Tian\****Page No. – Page No.****Redox Responsive Fluorescent nanoparticles based on Diselenide-containing AIEgens for Cell imaging and Selective Cancer Therapy**

We reported AIEgens containing diselenide bond, which could co-assemble with prodrug into nanoparticles. The self-assembly driving forces were explored by molecular dynamics (MD) simulations. The NPs could be cracked in the cancer intracellular environment that could be applied for bioimaging and cancer therapy.